RSC Advances

PAPER

View Article Online
View Journal | View Issue

Cite this: *RSC Adv.*, 2020, **10**, 11966

Pulse electrochemical synthesis of polypyrrole/graphene oxide@graphene aerogel for high-performance supercapacitor†

Erhui Zhang,[ab] Weifeng Liu,[ac] Xuguang Liu,*[ac] Zongbin Zhao[d] and Yongzhen Yang*[a]

A novel electroactive polypyrrole/graphene oxide@graphene aerogel (PGO@GA) was synthesized for the first time by pulse electropolymerization. The off-time in this technique allows polypyrrole (PPy) to go through a more stable structural arrangement, meanwhile its electronic transmission performance is enhanced by immobilizing graphene oxide between PPy chains. Moreover, graphene aerogel provides a three-dimensional structure with high conductivity to protect PPy from swelling and shrinking during the capacitive testing. Under these synergistic effects, PGO@GA presents exceptional capacitive performances including high specific capacitance (625 F g^{-1} at 1 A g^{-1}), excellent rate capability (keeping 478 F g^{-1} at 15 A g^{-1} with retention rate of 76.5%), and excellent cycling life (retaining 85.7% of its initial value when cycling 5000 times at 10 A g^{-1}). Therefore, the strategy adopted by this research provides a good reference for preparing other PPy-based electrode materials applied in the fields of catalysis, sensing, adsorption and energy storage.

Received 7th January 2020
Accepted 10th March 2020

DOI: 10.1039/d0ra01181a

rsc.li/rsc-advances

Polypyrrole (PPy), a widely-used conducting polymer, holds huge application potential in sewage disposal,[1] extraction of precious metals,[2] catalysts,[3] sensing[4] and energy storage,[5] owing to its advantages including superior biocompatibility, relatively high conductivity, high electrochemical activity and low preparation cost.[6] Together with its excellent pseudocapacitive properties, PPy usually acts as an outstanding electrode material applied in the field of supercapacitors. However, there still exist some defects in pure PPy because its chains suffer from serious swelling and shrinking during the charge–discharge process, which in turn severely weakens the rate capability and cycling life of supercapacitors.[7]

Pulse electropolymerization, compared with the method of constant potential[8] or galvanostatic deposition,[9] can regulate on-off time, pulse cycles and work potential to make pyrrole monomers continually polymerized into PPy on new active sites, and meanwhile to allow newly-formed PPy have enough time of experiencing structural rearrangement to improve its structural stability and electrochemical activity.[10] For the sake of further overcoming the intrinsic flaws of pure PPy and developing its potentials, up to now, various PPy-based composites have been designed. For instance, some groups have realized the improvement of electronic transport property of PPy[11,12] by incorporating graphene oxide with large-size anion nature into PPy chains. Singu and Yoon developed a novel ternary composite (GO–PPy–Ag)[13] exhibiting high specific capacitance (277.5 F g^{-1} at 2 A g^{-1}) and superior cycle life (keeping 93% after cycling 5000 charge–discharge at 2 A g^{-1}). Apart from these cases, graphene, owing to its exceptional conductivity, large theoretical specific surface area and excellent chemical stability,[14] has always been the most acceptable material employed to functionalize PPy for integrating their respective advantages. For instance, Ma *et al.*[15] synthesized polypyrrole/bacterial cellulose/graphene by a combination of *in situ* polymerization and filtering method, and the obtained nanomaterial exhibited a high areal capacitance of 3.66 F cm^{-2} at 1 mA cm^{-2}. Nevertheless, the inherent advantages of graphene are far from being full developed owing to serious restacking of graphene sheets caused by the enhanced π–π interaction during chemical or electrochemical reduction of GO.[16]

Graphene aerogel, as one emerging material, is synthesized by self-assembly of graphene sheets in different crosslinking ways.[17] The crosslinks not only restrain the restacking of graphene sheets efficiently but also initiate the formation of hierarchical pores that can shorten transport route of ions. Together

[a]*Key Lab of Interface Science and Engineering in Advanced Materials (Taiyuan University of Technology), Ministry of Education, Taiyuan 030024, China. E-mail: liuxuguang@tyut.edu.cn; yyztyut@126.com*

[b]*College of Chemistry and Chemical Engineering, Taiyuan University of Technology, Taiyuan 030024, China*

[c]*Institute of New Carbon Materials, Taiyuan University of Technology, Taiyuan 030024, China*

[d]*Carbon Research Laboratory, Liaoning Key Lab for Energy Materials and Chemical Engineering, State Key Lab of Fine Chemicals, School of Chemical Engineering, Dalian University of Technology, Dalian 116023, China*

† Electronic supplementary information (ESI) available. See DOI: 10.1039/d0ra01181a

with its excellent conductivity, graphene aerogel can serve as an excellent conductive matrix[18] to support the electrochemical deposition of PPy.

In this research, polypyrrole/graphene oxide@graphene aerogel (PGO@GA) nanocomposite was designed and constructed, which achieves a more enhanced capacitive performance than PPy owing to the modification of GO and graphene aerogel. The structure–activity relationship between components, morphologies and capacitive performances for this ternary composite was discussed on the basis of a series of structural characterization and electrochemical test.

The synthesis route of PGO@GA is illustrated in Fig. 1. First, the working electrode is prepared by coating method. Then it is immersed in electrolyte containing pyrrole monomer, GO and KCl (acting as supporting electrolyte). As is well known, GO dissolved in aqueous solution always carries negative charge owning to ionization of carboxyl and phenolic hydroxyl groups on GO.[19] At work potential, pyrrole monomers are oxidized into PPy whose chains carry positive electricity to attract negatively charged GO onto them. At the subsequent open circuit potential, the circulating current is cut off so that the oxidation polymerization reaction stops and meanwhile the relatively long off-time promotes diffusion of pyrrole monomers towards reactive boundary layer on electrode surface to form new active sites, where pyrrole monomers constantly grow into PPy at the next work potential, accompanied with the continuous doping of ionized GO sheets. Going through such a recurrent pulse electropolymerization process, PGO@GA is formed.

Fig. 2 exhibits the FTIR spectra of GO, PPy, PGO and PGO@GA. For GO, the bands at 1731, 1610 and 1056 cm^{-1} correspond to stretching vibration of C=O, graphitic C=C and C–O–C (alkoxy group), respectively.[20] As for PPy, the bands at 1541 and 1460 cm^{-1} correspond to the symmetric and asymmetric stretching vibrations of pyrrole ring.[21] The band located at 1295 cm^{-1} is related with the in-plane vibration of =C–H while that at 1037 cm^{-1} is attributed to C–H deformation vibration.[22,23] The bands at 963 and 773 cm^{-1} indicate the formation of polymerized pyrrole, meanwhile, the bands at

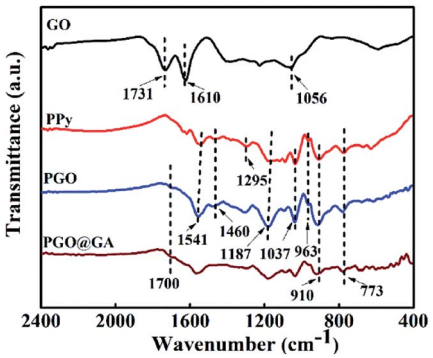

Fig. 2 FTIR spectra of GO, PPy, PGO and PGO@GA.

1187 and 910 cm^{-1} imply the doping state of PPy.[24] It is worth noting that all the bands of PPy also appear in PGO and PGO@GA, proving the introduction of PPy. Apart from that, the band ascribed to the C=O group of GO downshifts to 1700 cm^{-1} for PGO and PGO@GA because of the π–π interaction and the hydrogen bonding produced between GO layers and aromatic polypyrrole rings,[25] proving that carboxyl group plays an important role when GO is immobilized into PPy chains.

It can be observed from SEM images, as shown in Fig. 3(a–c), that GA exhibits three-dimensional network structure consisting of graphene sheets with highly wrinkled and chiffon-like features. As shown in Fig. S1 and S2,† the morphology and specific capacitance of PPy vary as a function of pulse cycle. It can be observed that PPy prepared at pulse cycles of 1000 obtains the highest specific capacitance (453 F g^{-1}), owing to its smooth micromorphology (Fig. 3d–f) that facilitates the electron mobility,[26] and the mass of PPy deposited on carbon cloth

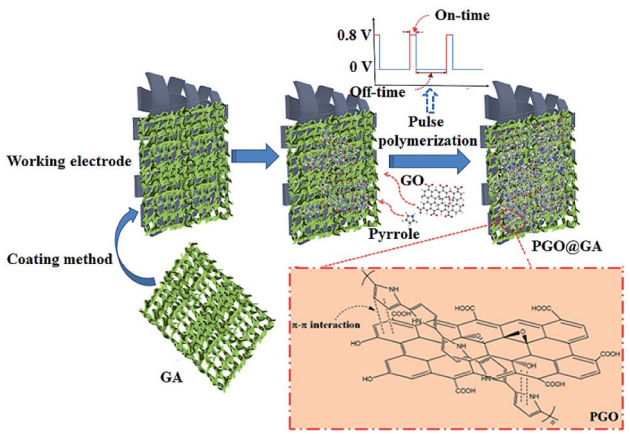

Fig. 1 Pulse electropolymerization technique for synthesis of PGO@GA.

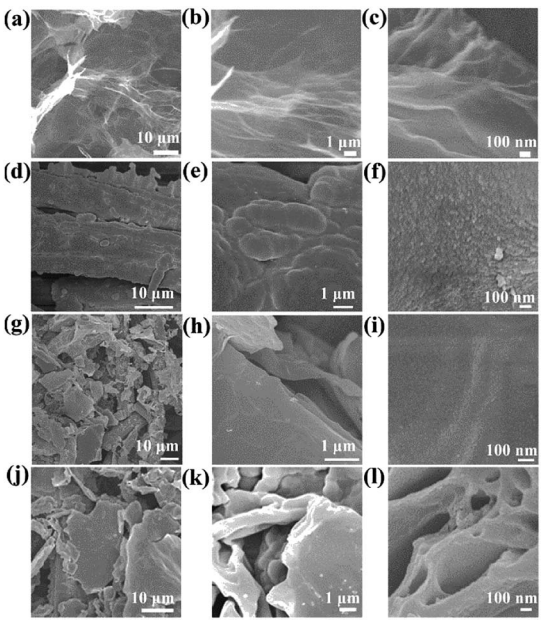

Fig. 3 SEM images of samples at different magnifications. (a–c) GA, (d–f) PPy, (g–i) PGO, (j–l) PGO@GA.

(19.2 mg) is about 4.8 mg. By contrast, the mass of PPy at pulse cycles of 500, 1500, 2000, 2500 and 3000 achieves 2.6, 9.6, 10.6, 14.9 and 17.8 mg respectively. Therefore, it can be evaluated that the PPy film gets much thicker as the increase of pulse cycles and pulse cycles are set as 1000 to prepare PGO and PGO@GA. Compared with pure PPy, PGO obtains a smoother microstructure (Fig. 3g–i) owing to the introduction of GO, which endows PGO with higher electrochemical activity than PPy. It can be observed from Fig. 3j–l that PGO@GA exhibits a coral-like structure, on which flat polymer layers are distributed.

At excitation wavelength of 532 nm, the G peak of single and double layers of graphene is located at 1614 and 1608 cm^{-1} respectively.[27] Based on interpolation method,[28] the stacked graphene layers of PGO@GA, whose G peak is at 1584 cm^{-1} (Fig. S3b†), are about 6. As is well known, thickness of a single layer of graphene is around 1 nm,[29] therefore, the thickness of stacked graphene in void pore wall is ~6 nm. It can be tested from Fig. 3l that thickness of void pore wall is ~14 nm, accordingly, the thickness of PPy deposited on GA is about 8 nm.

The structures of GO, PPy, PGO and PGO@GA were analyzed by XRD and Raman. Two peaks centered at $2\theta = 10.9°$ and 21.7° correspond to the (001) plane and (002) plane of GO, respectively (Fig. S3a†). The broad peaks located at $2\theta = 25.3°$ (3.5 Å) for PPy, PGO and PGO@GA are associated with the closest distance between the planar aromatic rings of pyrrole, like face-to-face pyrrole rings.[30,31] Except for PPy, diffraction peak for (001) crystal face of GO at $2\theta = 10.9°$ also appears on PGO and PGO@GA, indicating the introduction of GO into these two materials.

In the Raman spectra (Fig. S3b†), as for PPy, the peak located at 1571 cm^{-1} is due to C=C backbone stretching.[32] The double peaks situated at 1230 and 1320 cm^{-1} are attributed to the ring-stretching mode of PPy and another double peaks at 1041 and 979 cm^{-1} mainly come down to the C–H in-plane deformation.[33] However, these peaks belonging to PPy disappears in PGO and PGO@GA composites except for the slightly up-shifted D band approaching the peak of PPy at 1320 cm^{-1}. It can be speculated that the immobilization of GO into PPy chains results in the change in molecular vibration and rotation of PPy.

The elemental constituents of samples were analyzed using XPS (Fig. S4†). It is worth noting that the atomic percentage content of oxygen increases successively from PPy, PGO to PGO@GA (Fig. S4a†), which is attributed to the functionalization of PPy by GO and GA. The relatively high oxygen content in PPy mainly results from its molecular conformation optimization during the pulse electropolymerization process,[26] which facilitates the diffusion of water to form hydroxyl radical for nucleophilic attack towards PPy. What is more important is that the high oxygen contents endow these materials with excellent hydrophilicity favourable for lowering the transmission resistance of electrolyte and thus forming large reactive interface area. It is observed from Fig. S4b† that only pyrrolic N[34] exists, accompanied with bonding energy differences among them, which can be explained by the generated electron transfer between PPy, GO and GA. The elemental mappings reveal that carbon, nitrogen, and oxygen elements coexist and are distributed over the sheets (Fig. S5†), demonstrating the hybrid structure.

The capacitive performances of PPy, PGO and PGO@GA were investigated in 1.0 M KCl by using cyclic voltammetry (CV), galvanostatic charge–discharge (GCD) and electrochemical impedance spectroscopy (EIS). It can be seen from Fig. 4a that CV curves of PPy, PGO and PGO@GA at 5 mV s^{-1} all exhibit quasi-rectangular shapes, demonstrating ideal electrical double-layer capacitor (EDLC) behaviors at electrode–electrolyte interface.[35] Apart from that, the closure area of CV curve for PPy, PGO and PGO@GA increases successively, indicating elevated specific capacitance in turn. That is due to the following reasons: (1) the negatively charged GO immobilized into PPy chains must be balanced by cation ingression from electrolyte, which contributes to a higher current density in the negative potential region[25] and the involved reaction mechanism can be described as: $PPy^{+}/GO^{-} + K^{+} + e \leftrightarrow PPy^{0}/GO^{-}/K^{+}$;[36] (2) the coral-like network with superior conductivity for GA not only shortens transmission path of ions in electrolyte and accelerates electron transfer but also protects PPy from structural deformation.

Similar tendency can be also seen from Fig. 4b. All GCD curves present quasi-isosceles triangle, indicating that the capacitance mainly comes from the EDLC properties of materials in neutral electrolyte. The capacitance value for PPy, PGO and PGO@GA at 1 A g^{-1} achieves 453, 514 and 625 F g^{-1}, respectively.

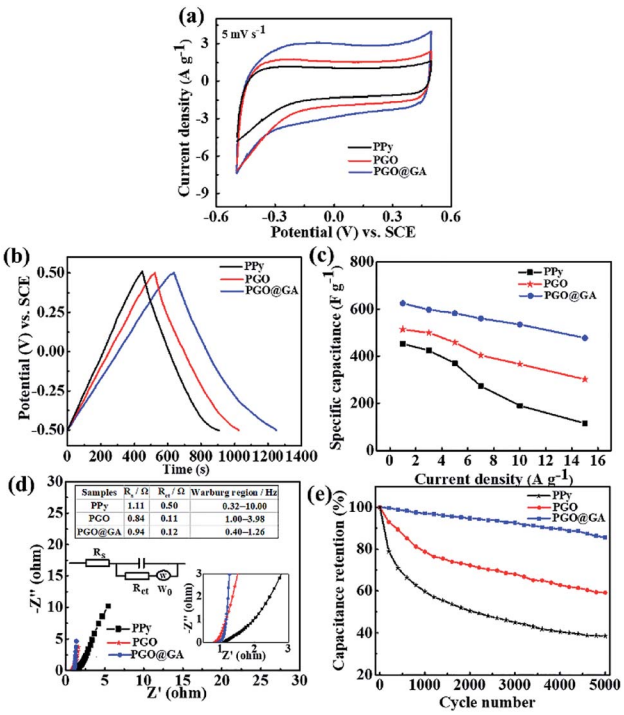

Fig. 4 Capacitive properties of samples in 1.0 M KCl: (a) CV curves at 5 mV s^{-1}; (b) GCD profiles at 1 A g^{-1}; (c) capacitance values at current densities ranging from 1 to 15 A g^{-1}; (d) Nyquist plots of PPy, PGO, PGO@GA, and the equivalent circuit used to fit EIS results (inset); (e) cycling stability of PPy, PGO, PGO@GA at a current density of 10 A g^{-1}.

The capacitance for PPy, PGO and PGO@GA corresponding to the current densities ranging from 1 to 15 A g^{-1} was investigated and the results are shown in Fig. 4c. It can be observed that specific capacitance of PGO@GA still achieves 478 F g^{-1} even at high current density of 15 A g^{-1} with a relatively high capacitance retention rate of 76.5%, which is obviously higher than those of PGO (58.7%) and PPy (25.2%), demonstrating that the synergistic effect among GO, PPy and GA promotes the rate capability of PGO@GA.

EIS analysis of PPy, PGO and PGO@GA was conducted to detect their charge transfer resistance and ion diffusion rate, and the results are presented in Fig. 4d. Based on the equivalent circuit, the intercept with the real impedance axis in the high-frequency region represents equivalent series resistance R_s, including contact resistance, intrinsic resistance of electrode materials and solution resistance.[37] The diameter of the semicircle in medium-frequency region symbolizes charge-transfer resistance (R_{ct}). As proved in M. Deng *et al.*'s reports,[11] electron transmission ability of PPy is improved owing to the introduction of GO between PPy chains. Moreover, X. Du *et al.*'s research[26] also demonstrates that point based on the reduced R_{ct}. Therefore, similar conclusion can be drawn from the fitted results illustrated in Fig. 4d that R_s and R_{ct} values for PGO and PGO@GA get lower than those of PPy after PPy goes through the functional modification of GO and GA.

The Warburg region refers to the section of curve with 45° slope, corresponding to the intermediate frequency range. The shorter the frequency range gets, the better ion diffusion capability the material exhibits. Therefore, it can be concluded from the fitted results in Fig. 4d that the modification of GO, GA and pulse regulation for PPy realizes the optimum ion diffusion for PGO@GA.

In addition, compared with the curve of PPy and PGO in low-frequency region, that for PGO@GA is closer to parallel with imaginary axis, which implies its more ideal EDLC behaviors.

It can be seen from the cyclic stability test (Fig. 4e) that the capacitance retention for PGO@GA achieves 85.7% even undergoing 5000 cycles at 10 A g^{-1}, higher than that for PPy (38.5%) and PGO (59.2%).

Most of the reported materials listed in Table S1† are prepared by non-pulse deposition techniques. These electrode materials fail to achieve high specific capacitance as well as excellent capacitance stability simultaneously, which is mainly attributed to the serious swelling and shrinking of polypyrrole during charge–discharge process. By contrast, a combination of pulse regulation, modification of GO and protection of GA towards PPy endows PGO@GA with smooth porous microstructure and enhances structural stability of PPy, which facilitates electron mobility and electrolyte transport. Therefore, PGO@GA enjoys higher capacitance stability even after 5000 charge–discharge cycles at the high current density of 10 A g^{-1}, besides, the material also obtains a higher mass specific capacitance at 1 A g^{-1}.

It can be concluded from all the above electrochemical performance test results that PGO@GA electrode holds optimum capacitance performance, which is attributed to the following reasons: (1) during pulse electropolymerization, PPy experiences more stable structural rearrangement to endow it with improved electrochemical activity; (2) large-sized GO with anionic attribute is immobilized into PPy to optimize its electron transport property and structural stability; (3) GA provides three-dimensional network with good conductivity supporting anisotropic deposition of pyrrole monomer and GO, which not only generates large number of active sites of electrochemical reaction but shortens ion transport paths and inhibit the swelling and shrinking of polypyrrole also during charge–discharge process.

In conclusion, the synthetic PGO@GA by pulse electropolymerization technique exhibits high specific capacitance (625 F g^{-1}) at 1 A g^{-1} and still retains 478 F g^{-1} even at a high current density of 15 A g^{-1} with superior capacitance retention rate of 76.5%. Moreover, excellent cycling life (retaining 85.7% of its initial value when cycling 5000 times at 10 A g^{-1}) for PGO@GA is also obtained. The outstanding capacitance behavior benefits from multiplexed conduction channel from GA and the enhanced structural stability and electrochemical activity of PPy. It is expected that the improved modification strategy for PPy provided by this research will be a good reference to synthesize other types of PPy-based nanomaterial by regulating the categories of anions and conductive matrix to realize applications in established fields.

Conflicts of interest

There are no conflicts to declare.

Acknowledgements

This work was supported by the National Key Research and Development Program of China (2017YFB0603104); National Natural Science Foundation of China (U1610255, U1607120, 51603142, 21706170, 5190222); Key Research and Development Program International Cooperation Project of Shanxi Province (201903D421077); Shanxi Provincial Key Innovative Research Team in Science and Technology (201605D131045-10).

Notes and references

1 Y. H. Lin, X. L. Cui and J. Bontha, *Environ. Sci. Technol.*, 2006, **40**, 4004–4009.
2 X. Du, G. Guan, X. Li, A. D. Jagadale, X. Ma, Z. Wang, X. Hao and A. Abudula, *J. Mater. Chem. A*, 2016, **4**, 13989–13996.
3 M. Góral-Kurbiel, A. Drelinkiewicz, R. Kosydar, B. Dembińska, P. Kulesza and J. Gurgul, *Electrocatalysis*, 2014, **5**, 23–40.
4 T. Qian, S. Wu and J. Shen, *Chem. Commun.*, 2013, **49**, 4610–4612.
5 R. Sun, H. Chen, Q. Li, Q. Song and X. Zhang, *Nanoscale*, 2014, **6**, 12912–12920.
6 S. Yan, Q. Yang, G. Han, Q. Wang, X. Li, L. Wang, Z. Luo, R. You and Q. Zhang, *New J. Chem.*, 2019, **43**, 2559–2566.
7 Y. Song, T. Y. Liu, X. X. Xu, D. Y. Feng, Y. Li and X. X. Liu, *Adv. Funct. Mater.*, 2015, **25**, 4626–4632.
8 Y. S. Lim, Y. P. Tan, H. N. Lim, W. T. Tan and M. A. Yarmo, *J. Appl. Polym. Sci.*, 2013, **128**, 224–229.

9 M. Porcher, C. Esnault, F. O. Tran-Van and F. Ghamouss, *J. Appl. Electrochem.*, 2016, **46**, 1–13.
10 A. Davies, P. Audette, B. Farrow, F. Hassan and A. Yu, *J. Phys. Chem. C*, 2011, **115**, 17612–17620.
11 M. Deng, X. Yang, M. Silke, W. Qiu, M. Xu, G. Borghs and H. Chen, *Sens. Actuators, B*, 2011, **158**, 176–184.
12 A. Österholm, T. Lindfors, J. Kauppila, P. Damlin and C. Kvarnström, *Electrochim. Acta*, 2012, **83**, 463–470.
13 B. S. Singu and K. R. Yoon, *Electrochim. Acta*, 2018, **268**, 304–315.
14 Z. Fan, J. Zhu, X. Sun, Z. Cheng, Y. Liu and Y. Wang, *ACS Appl. Mater. Interfaces*, 2017, **9**, 21763–21772.
15 L. Ma, R. Liu, H. Niu, F. Wang, L. Liu and Y. Huang, *Electrochim. Acta*, 2016, **222**, 429–437.
16 X. Díez-Betriu, F. J. Mompeán, C. Munuera, J. Rubio-Zuazo, R. Menéndez, G. R. Castro and A. de Andrés, *Carbon*, 2014, **80**, 40–49.
17 H. L. Gao, Y. B. Zhu, L. B. Mao, F. C. Wang, X. S. Luo, Y. Y. Liu, Y. Lu, Z. Pan, J. Ge, W. Shen, Y. R. Zheng, L. Xu, L. J. Wang, W. H. Xu, H. A. Wu and S. H. Yu, *Nat. Commun.*, 2016, **7**, 12920.
18 Z. Xu, Y. Zhang, P. Li and C. Gao, *ACS Nano*, 2012, **6**, 7103–7113.
19 S. Stankovich, D. A. Dikin, R. D. Piner, K. A. Kohlhaas, A. Kleinhammes, Y. Jia, Y. Wu, S. T. Nguyen and R. S. Ruoff, *Carbon*, 2007, **45**, 1558–1565.
20 X. Yang, M. Xu, W. Qiu, X. Chen, M. Deng, J. Zhang, H. Iwai, E. Watanabe and H. Chen, *J. Mater. Chem.*, 2011, **21**, 8096–8103.
21 Y. Liu, Y. Zhang, G. Ma, Z. Wang, K. Liu and H. Liu, *Electrochim. Acta*, 2013, **88**, 519–525.
22 J. Cao, Y. Wang, J. Chen, X. Li, F. C. Walsh, J. H. Ouyang, D. Jia and Y. Zhou, *J. Mater. Chem. A*, 2015, **3**, 14445–14457.
23 X. Zhang, J. Zhang, W. Song and Z. Liu, *J. Phys. Chem. B*, 2006, **110**, 1158–1165.
24 J. Zhang and X. S. Zhao, *J. Phys. Chem. C*, 2012, **116**, 5420–5426.
25 C. Zhu, J. Zhai, D. Wen and S. Dong, *J. Mater. Chem.*, 2012, **22**, 6300–6306.
26 X. Du, X. Hao, Z. Wang, X. Ma, G. Guan, A. Abuliti, G. Ma and S. Liu, *Synth. Met.*, 2013, **175**, 138–145.
27 A. C. Crowther, A. Ghassaei, N. Jung and L. E. Brus, *ACS Nano*, 2012, **6**, 1865–1875.
28 P. Chen, A. Quarteroni and G. Rozza, *ESAIM: Math. Modell. Numer. Anal.*, 2014, **48**, 943–953.
29 H. Bai, C. Li and G. Shi, *Adv. Mater.*, 2011, **23**, 1089–1115.
30 G. R. Mitchell, *Polym. Commun.*, 1986, **27**, 346–349.
31 Y. C. Liu and T. C. Chuang, *J. Phys. Chem. B*, 2003, **107**, 12383–12386.
32 T. Qian, C. Yu, S. Wu and J. Shen, *J. Mater. Chem. A*, 2013, **1**, 6539–6542.
33 Y. Shi, L. Pan, B. Liu, Y. Wang, Y. Cui, Z. Bao and G. Yu, *J. Mater. Chem. A*, 2014, **2**, 6086–6091.
34 L. Chen, R. Du, J. Zhu, Y. Mao, C. Xue, N. Zhang, Y. Hou, J. Zhang and T. Yi, *Small*, 2015, **11**, 1423–1429.
35 B. Fang and L. Binder, *J. Power Sources*, 2006, **163**, 616–622.
36 G. Lian and S. Dong, *J. Electroanal. Chem.*, 1989, **260**, 127–136.
37 M. Li, C. Liu, H. Cao, H. Zhao, Y. Zhang and Z. Fan, *J. Mater. Chem. A*, 2014, **2**, 14844–14851.